PHYSICAL REVIEW D **71,** 124005 (2005)

Choptuik's scaling in higher dimensions

Evgeny Sorkin* and Yonatan Oren†

Racah Institute of Physics, Hebrew University, Jerusalem 91904, Israel

(Received 14 February 2005; published 3 June 2005)

We extend Choptuik's scaling phenomenon found in general relativistic critical gravitational collapse of a massless scalar field to higher dimensions. We find that in the range $4 \leq D \leq 11$ the behavior is qualitatively similar to that discovered by Choptuik. In each dimension we obtain numerically the universal numbers associated with the critical collapse: the scaling exponent γ and the echoing period Δ. The behavior of these numbers with increasing dimension seems to indicate that γ reaches a maximum and Δ a minimum value around $11 \leq D \leq 13$. These results and their relation to the black hole–black string system are discussed.

DOI: 10.1103/PhysRevD.71.124005 PACS numbers: 04.50.+h, 04.25.Dm, 04.70.Bw

I. INTRODUCTION

General relativity (GR) in higher dimensions ($D > 4$) has been receiving increasing attention in recent years. This is largely motivated by the phenomenological ''brane-world'' and ''large-extra-dimensions'' scenarios that are rooted in string theory, which is intrinsically higher dimensional, involving 10 or 11 dimensions. But regardless, GR in itself does not favor the 4D case especially; rather it is independent of the dimension, and so without any additional reasons the dimension of spacetime may and should be considered a *parameter* of the theory.

Adopting this point of view, one finds that certain properties and solutions of GR change qualitatively in higher dimensions. In particular, black hole uniqueness breaks down in $D > 4$. This implies the existence of black objects with nonspherical horizon topologies. Examples include the caged black hole/black string system in a spacetime with compact extra dimensions, see [1] for a review, and the rotating black hole/black ring configurations [2,3]. The phase transitions between different horizon topologies seem to lead to a compromise of cosmic censorship in higher dimensions and to be accompanied by energy outbursts (see e.g. [4]). Moreover, there exist *critical dimensions* above which the qualitative properties of the spoken phase transition change [5–7].[1]

In this paper we study the critical collapse of a spherically symmetric massless scalar field in D-dimensional spacetime, in search of similar nontrivial dimensional effects. The critical behavior of black hole formation is a striking example of the surprising phenomena to be found in gravitational physics. It is understood that in the dynamical gravitational collapse of matter fields, initial configurations with very low density will usually disperse to infinity, while extremely dense clumps will collapse to form a black hole. What happens in the intermediate case between these two extremities is much less obvious. In 1992, Choptuik [9] studied this limiting case numerically, modeling the collapsing matter as a spherically symmetric configuration of massless scalar field coupled to gravity. For each family of initial data (e.g. Gaussian, Lorentzian, etc.), parameterized by an amplitude p, there is a critical amplitude p_*. If $p > p_*$ the final state is a black hole (supercritical collapse), otherwise the field disperses leaving behind empty flat space (subcritical collapse). The following discoveries were made regarding the behavior of this system near the threshold amplitude p_* in 4D:

(i) In supercritical collapse arbitrarily small black holes are formed as $p \to p_*$. In this limit the black hole mass M scales as $M \propto (p - p_*)^\gamma$, with the prefactor and p_* characteristic of the specific family of initial data. The exponent, however, is universal and independent of the shape of initial data. Its numerical value is $\gamma \simeq 0.374$. Later it also was discovered that in subcritical collapse the maximal scalar curvature encountered before the field disperses scales as $R_{\max} \propto (p_* - p)^{-2\gamma}$ [10].

(ii) The critical solution itself is universal. Namely, following a short transient stage, the spacetime converges to a universal solution independent of the initial data, remains such for a while, and then either collapses or disperses, depending on whether $p > p_*$ or not.

(iii) The critical solution is discretely self-similar. Designating the critical solution (collectively for the scalar field and the metric) by $Z_*(r, t)$, this means that $Z_*(r, t) = Z_*(re^\Delta, te^\Delta)$, with the empirically found $\Delta \simeq 3.44$. The field and metric functions pulsate periodically with ever decreasing temporal and spatial scales, until a singularity is formed at the accumulation point, $r = t = 0$.

*Electronic address: sorkin@phys.huji.ac.il
†Electronic address: yono@phys.huji.ac.il

[1] Another example of the qualitative dependence of GR on dimension is the chaotic behavior of the spacetime near a spacelike singularity, discovered by Belinskii, Khalatnikov and Lifshitz. Specifically, above the critical dimension $D_{\mathrm{BKL}} = 10$, the system becomes nonchaotic, see the recent review [8].

Similar results also were observed for other kinds of matter and extensive literature has been written on the subject. For a review see [11] and the references therein.[2]

There are several reasons why we find it interesting to explore the critical phenomena in higher dimensions: (i) The mysterious universal numbers that appear in critical collapse, such as the scaling exponent and the echoing period, are known only empirically. One may wonder if it is possible to use the *dimension as a probe* that can provide insights or hints into the origin of these numbers; (ii) The Choptuik critical phenomena, or more precisely its time-symmetric version, is related to the phase transition in the black string/black hole system [14]. It might be possible to learn about the behavior of that system near the merger point where the topology changes from that of a black string to that of a black hole by better understanding the higher-dimensional critical collapse scenario; (iii) The massless scalar field collapse is probably the simplest model of dynamical collapse in GR. It is worthwhile to understand what kind of new features one can expect to find there in higher dimensions.

To realize these goals we designed a numerical code that evolves the spacetime and scalar field equations and allows us to study the critical solution in different dimensions. As is often the case in numerical analysis, we encountered unexpected problems that demanded special treatment. In addition to the familiar methods used in 4D like ''constrained'' evolution and mesh refinement, the code uses analytical series expansion near the origin and ''synthetic friction'' (or ''smoothing'') to handle the severe divergences appearing in higher dimensions. We employed this code for $4 \leq D \leq 11$.

In all our simulations we find that the near-critical collapse proceeds in the discretely self-similar (DSS) manner as in the 4D case. For each dimension we obtain the (logarithmic) period of the pulsations Δ and the scaling exponent γ, which we define such that the dimension of length is $[\text{length}] \propto |p - p_*|^\gamma$. These results are summarized in Table I. In the examined range of dimensions we find that Δ decreases and γ increases[3] with D. While we could not check this explicitly, since our numerical tools did not take us further than $D = 11$, we were tempted to extrapolate our results beyond that. This *extrapolation* seems to indicate that Δ reaches a minimum and γ has a maximum somewhere in between $11 \leq D \leq 13$, see Figs. 10 and 11. In any case, the dimensional dependence of these variables is smooth (apparently lacking in divergences). Moreover, γ varies slowly with respect to D, and the critical exponent for mass in D dimensions is $\gamma_{\text{mass}} = (D - 3)\gamma$, so as the dimension grows the mass of a black hole forming above the threshold increases steeply with $p - p_*$.

TABLE I. The echoing period of the scalar field Δ and the scaling exponent γ in different dimensions. The error in Δ represents the variation about the mean Δ measured on several periods of oscillation. The error in γ originates both from the linear fitting and from the actual numerical errors in the measured scalar curvature. However it has been verified by convergence analysis that the dominant error is in the fitting. The values of Δ and γ that we find for $D = 4, 6$ agree well with the numbers found in the literature.

D	Δ	γ
4	$3.37 \pm 2\%$	$0.372 \pm 1\%$
5	$3.19 \pm 2\%$	$0.408 \pm 2\%$
6	$3.01 \pm 2\%$	$0.422 \pm 2\%$
7	$2.83 \pm 2\%$	$0.429 \pm 2\%$
8	$2.70 \pm 3\%$	$0.436 \pm 2\%$
9	$2.61 \pm 3\%$	$0.442 \pm 2\%$
10	$2.55 \pm 3\%$	$0.447 \pm 3\%$
11	$2.51 \pm 3\%$	$0.44 \pm 3\%$

In the next section we formulate our problem: we derive the equations and define the variables. Then in Sec. III we describe our numerical scheme. The results are presented in Sec. IV. These and their relation to the black hole/black string system is discussed in Sec. V. In the same section we state some open questions.

II. EQUATIONS AND VARIABLES

We turn now to formulate the physical problem at hand. In spherical symmetry, we describe the D dimensional asymptotically flat spacetime in double-null coordinates (u, v) by the metric:

$$ds^2 = -\alpha(u, v)^2 du dv + r(u, v)^2 d\Omega_{D-2}^2, \tag{1}$$

where $d\Omega_{D-2}^2$ is the metric on a unit $\mathbf{S}^{D-2}$ sphere and the axis $r = 0$ is chosen to be where $u = v$.

The action of the massless scalar field ϕ minimally coupled to gravity in D dimensions is given by

$$S = \frac{1}{16\pi G} \int R\sqrt{-g} d^D x - \int g^{ab} \partial_a \phi \partial_b \phi \sqrt{-g} d^D x. \tag{2}$$

The Einstein equations, $R_{ab} = 8\pi G \phi_{,a} \phi_{,b}$ derived from this action under the metric (1) are

$$r_{,uv} + (D - 3)\frac{r_{,u} r_{,v} + \alpha^2/4}{r} = 0, \tag{3}$$

[2]While a majority of authors do not go beyond 4D, Garfinkle *et al.* [12] have obtained γ and Δ in 6D and Birukou *et al.* [13] got γ in the critical scalar field collapse in 5D and 6D.

[3]There is some decrease in γ for $D = 11$ but we cannot definitely determine if this reflects a physical behavior or is caused by the escalation of numerical errors in higher dimensions.

$$\frac{\alpha_{,uv}}{\alpha} - \frac{\alpha_{,u}\alpha_{,v}}{\alpha^2} - \frac{(D-2)(D-3)}{2}\frac{r_{,u}r_{,v} + \alpha^2/4}{r^2} + 4\pi G\phi_{,u}\phi_{,v} = 0, \quad (4)$$

$$r_{,uu} - 2\frac{\alpha_{,u}}{\alpha}r_{,u} + \frac{8\pi G}{D-2}r\phi_{,u}^2 = 0, \quad (5)$$

$$r_{,vv} - 2\frac{\alpha_{,v}}{\alpha}r_{,v} + \frac{8\pi G}{D-2}r\phi_{,v}^2 = 0, \quad (6)$$

where the first two are hyperbolic equations of motion, and the other two are constraints.

Variation of the action with respect to ϕ yields the scalar field equation of motion, $\Box\phi = 0$, which expands to

$$\phi_{,uv} + \frac{D-2}{2}\frac{\phi_{,u}r_{,v} + \phi_{,v}r_{,u}}{r} = 0. \quad (7)$$

Following Hamade and Stewart [15] we formulate the problem as a set of coupled first order differential equations. Designating $s \equiv \sqrt{4\pi G}\phi$ we define

$$D1:\ w \equiv s_{,u} \qquad D2:\ z \equiv s_{,v} \qquad D3:\ f \equiv r_{,u}$$
$$D4:\ g \equiv r_{,v} \qquad D5:\ d \equiv \frac{\alpha_{,v}}{\alpha}. \quad (8)$$

Then the complete set of evolution equations is

$$E1:\ f_{,v} + (D-3)\frac{fg + \alpha^2/4}{r} = 0,$$
$$E2:\ d_{,u} - \frac{(D-2)(D-3)}{2}\frac{fg + \alpha^2/4}{r^2} + wz = 0,$$
$$C1:\ f_{,u} - 2\frac{\alpha_{,u}}{\alpha}f + \frac{2}{D-2}rw^2 = 0,$$
$$C2:\ g_{,v} - 2dg + \frac{2}{D-2}rz^2 = 0,$$
$$S1:\ z_{,u} + \frac{D-2}{2}\frac{fz + gw}{r} = 0,$$
$$S2:\ w_{,v} + \frac{D-2}{2}\frac{fz + gw}{r} = 0.$$

Some useful scalar quantities include the Ricci scalar curvature, which is given by

$$R = -\frac{8wz}{\alpha^2}, \quad (9)$$

and the proper time of an observer at the axis,

$$T(u) = \int_0^u \alpha(u', u')du'. \quad (10)$$

The supercritical collapse of a spherical distribution of matter in D asymptotically flat dimensions results in the formation of a D-dimensional Schwarzschild-Tangherlini black hole, whose metric reads [16]

$$ds^2 = -f(r)dt^2 + f(r)^{-1}dr^2 + r^2d\Omega_{D-2}^2,$$
$$f(r) = 1 - (r_0/r)^{D-3}. \quad (11)$$

The ADM mass of the black hole is $M = (D-2)A_{D-2}r_0^{D-3}/(16\pi G)$ in terms of its Schwarzschild radius, r_0. $A_{D-2} \equiv 2\pi^{D/2-1}/\Gamma(D/2-1)$ is the area of a unit $\mathbf{S}^{D-2}$ sphere and G is the D-dimensional Newton constant.

We define the critical exponent γ such that $|p_* - p|^\gamma$ has dimensions of length. Then it follows [10,12] that in D dimensions the maximal curvature (having the dimension of inverse length squared) achieved in a subcritical collapse scales as $R_{\max} \propto (p_* - p)^{-2\gamma}$ and the mass of the black hole, forming in a supercritical collapse, behaves as $(p - p_*)^{\gamma_{\rm mass}}$ where $\gamma_{\rm mass} \equiv (D-3)\gamma$.

A. Initial data problem, gauge, and boundary conditions

We specify the initial scalar field profile along an outgoing null surface $u = u_i = \text{const}$, which we choose to be $u_i = 0$. To complete formulation of the initial value problem we note that the choice of metric (1) is only unique up to the redefinitions $v' = \chi(v)$, $u' = \xi(u)$. In order to fix this residual gauge freedom we choose the area coordinate r along the initial null surface $u = 0$ as $r = v/2$ (this is chosen to conform with the conventional definition of characteristic coordinates in flat space, $v = t + r$ and $u = t - r$). In addition, we set $\alpha = 1$ at the axis on $u_i = v = 0$. From here we can obtain all the other functions on the initial hypersurface by integration from the origin.

Equations $E1$–$E2$ and $S1$–$S2$ are singular at the axis. The physical solution is, however, perfectly regular there. This enforces the following boundary conditions on the scalar field and the metric functions along the axis $r = 0$

$$g = -f = \frac{1}{2}\alpha, \qquad w = z, \qquad \partial_r s = 0, \qquad \partial_r\alpha = 0. \quad (12)$$

The source terms which are singular at the axis are then evaluated by applying l'Hospital's rule.

The actual shape we choose for the initial configuration of the scalar field is a Gaussian shell

$$s(v, u = 0) = p\exp\left[-\left(\frac{v - v_c}{\sigma}\right)^2\right], \quad (13)$$

where v_c and σ are constants and the amplitude p is the aforementioned strength parameter of the initial data.

III. THE NUMERICAL SCHEME

Having laid out the framework, we proceed to describe the numerical solution of the above equations. We construct a grid in the u-v space as described in Fig. 1. The primitive computational cell is square, with grid spacings $h_v = h_u = h$. The initial ingoing wave is specified on an outgoing hypersurface of constant u, which is stored as a horizontal line in our grid, see Fig. 1 . Supposing we know the solution along an outgoing hypersurface $u - h$ then d and z are propagated to u using the equations $E2$ and $S1$

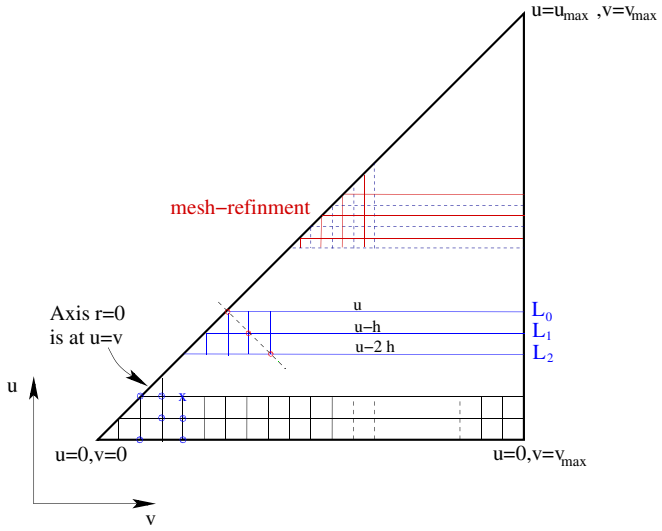

FIG. 1 (color online). The domain of integration. At any moment, in addition to the current outgoing hypersurface L_0, we keep two preceding levels L_1 and L_2. Boundary conditions involving $\partial/\partial r$ are implemented using three-point derivatives along the shown diagonal line. Mesh refinement is illustrated in the topmost rows. The smoothing of z (or d) near the axis at a point marked by a cross is done using the values of z (or d) at points on the past light cone of that point marked with circles.

correspondingly. Then we integrate the equations $S2$, $E1$, $C2$, $D2$, $D4$, and $D5$ from the axis outward along u to get w, f, g, s, r, and α, respectively. Note that we use what is called ''constrained evolution,'' namely, the constraint $C2$ is used in the evolution. This algorithm is iterated until either the domain of integration is entirely covered (in the subcritical case) or a black hole forms (in a supercritical collapse). The remaining equations are not used directly (but are used to determine the boundary conditions) in this scheme, but they must be satisfied by the solution. We monitor the equations $D3$ and $C1$ and verify that they are indeed satisfied to a prescribed precision during the evolution.

We use the fourth order Runge-Kutta algorithm to solve all equations. At every moment in addition to the solution along the line currently being solved (L_0 at u) we keep in memory the solution on the two preceding levels: L_1 at $u - h$ and L_2 at $u - 2h$. Without being too memory consuming, this makes the fourth order Runge-Kutta algorithm more elegantly applicable and also helps us to implement the axis boundary conditions as sketched in Fig. 1. The size of the domain is chosen such that the $v_{\max} = u_{\max}$ point is located just beyond the accumulation point.

A. Series expansion and smoothing near the axis

The basic scheme described above works well for collapse in $D = 4, 5$, but in higher dimensions the code becomes unstable. Moreover, for $D > 5$ this scheme is unstable even in *flat space*, where only the wave equations $S1 - S2$ are solved (with constant $g = -f = 1/2$). This instability clearly arises near the axis where r is small and the discretization errors in evaluating the sources are amplified. To illustrate what happens near the origin let us consider the wave equation $S2$ in flat space. Say we are solving for w along a $u = \text{const}$ ray at the grid point, labeled 1, next to the axis, labeled 0. First we rewrite the wave equation as $w_{,v} + [(D-2)/2]wr_{,v}/r = [(D-2)/4]z/r$, where we used the flat space value $f = -1/2$. Its formal solution is $w(v_1) = [(D-2)/4]/r^{D/2-1} \int_{v_0}^{v_1} r^{D/2-2} z(v')dv'$. Using e.g. trapezoidal rule we get

$$w_1 - w_0 = \frac{D-2}{8}\frac{h}{r_1}z_1 - z_0 + O(h^3), \qquad (14)$$

where we utilized the boundary condition (12), $w_0 = z_0$. Alternatively, approximating the integrand to linear order in h by Taylor series about 0 we evaluate the integral analytically to arrive at

$$w_1 - w_0 = \frac{D-2}{D}(z_1 - z_0) + O(h^2). \qquad (15)$$

Comparing (14) and (15) we learn that as D increases the first term in the right-hand side of (14) (where $r_1 = h/2$) grows linearly and dominates while the right-hand side in the analytical formula (15) barely varies. Hence the discrete version (14) overestimates w_1 by a factor[4] proportional to D, which clearly causes problems in higher dimensions.

We employ the series expansion method around the axis in equations $S2$ and $E1$ (the series expansion in $E1$ also averts error amplification in $E2$) such that the sources in these equations are evaluated at the axis. Then the propagation of z and d in the u direction is executed as before but with w and f obtained from the series expansion in all evaluations of sources, required by the Runge-Kutta algorithm. We determine the number of points near the origin where the series expansion is required empirically for every dimension. We found that optimally this number is approximately D points. (For example in $D = 8$ and for the initial grid spacing of 10^{-3} this is done at nine grid points.)

Unfortunately it turns out that while the series expansion prolongs the lifetime of the code before crashing, it is not enough to render it completely stable. After trying several other methods we ended up by adding an effective ''friction'' or smoothing in the u-propagated equations ($E2$ and $S1$). Specifically, the value of the function z (or d) at a point near the axis is mixed with values extrapolated from neighboring points on the past light cone of that point (see Fig. 1). Symbolically, the value of some function y

[4]Methods other than the trapezoidal rule can give another factor, which is still proportional to D, so for large D's the difference between the discrete and the analytical formulas increases anyway.

at the point marked by a cross in Fig. 1 is updated according to $y_x = [y_e + 3\omega \sum_{i=1}^{3} y_i]/(1 + 3\omega)$, where y_e is the value obtained from the evolution equation at the crossed point, and $y_i(u) = 2y(u - h) - y(u - 2h)$ are the extrapolated values along the three directions lying in the past light cone, designated by circles on the figure, and ω are the weights. The weights given to the values obtained from the evolution and from the extrapolation depend on D, but they are essentially comparable. (For the above $D = 8$ example the weights $\simeq 1$.) This procedure is in principle equivalent to adding a diffusive term in the evolution equations. The smoothing is applied at the same mesh points as the series expansion.

This series-smoothing symbiosis is a very stable method that satisfies the constraints $D3$ and $C1$. Its convergence rate, however, is less than quadratic but never below the linear. This is not a serious problem though. The typical run time of our code on a PC-class computer with satisfactory precision is on the order of minutes in spite of this relatively slow convergence. We use that series-smoothing method to obtain all the results reported in this paper.

B. Mesh refinement

Close to the threshold amplitude the solution becomes DSS, i.e. it is self-replicating on decreasing scales. In order to resolve this solution the grid spacing must be smaller than the smallest feature in the solution. A static grid with the spacing necessary for resolving several echoing periods will require a large amount of memory and computation time. This is very inefficient, and moreover unnecessary, because in the early stages the scales involved are still relatively large, so a very dense grid is superfluous to resolve them. This makes dynamical grid refinement imperative for a realistically feasible scheme. While there exist completely general adaptive mesh refinement techniques [17], we use a far simpler method proposed by Garfinkle [18].

The scheme relies on the fact that when u is incremented the grid point that lies on the axis [at $(v = u)$] enters the region $v < u$ and effectively leaves the causal past of the domain (see Fig. 1). Physically the ingoing ray is reflected from the origin and becomes an outgoing ray, but grid points which were assigned to it are lost. Thus the active part of the grid becomes smaller at large u, exactly when more resolution is needed for resolving the small features of the critical collapse. This unhappy situation can be prevented by interpolating the remaining points at $v > u$ back into the original array of points, restoring the original resolution. Following Garfinkle [18] we do this only when half of the grid points cross the axis. Since $v = u$ on the axis, we get a linear increase in the grid density and a linear decrease in h with u.

We use the code to calculate the spacetime near the critical solution in dimensions $4 \leq D \leq 11$. For each D we empirically locate the threshold amplitude p_* by a simple binary search until p_* is found with the desired accuracy, which is typically one part in $10^{10} - 10^{15}$ (the lowest is for $D = 11$). A typical grid has initially between 2000 and 8000 grid points in the initial outgoing surface. After several mesh refinements the step size h, initially of the order of 10^{-3} to 10^{-4}, is reduced by an order of magnitude or two.

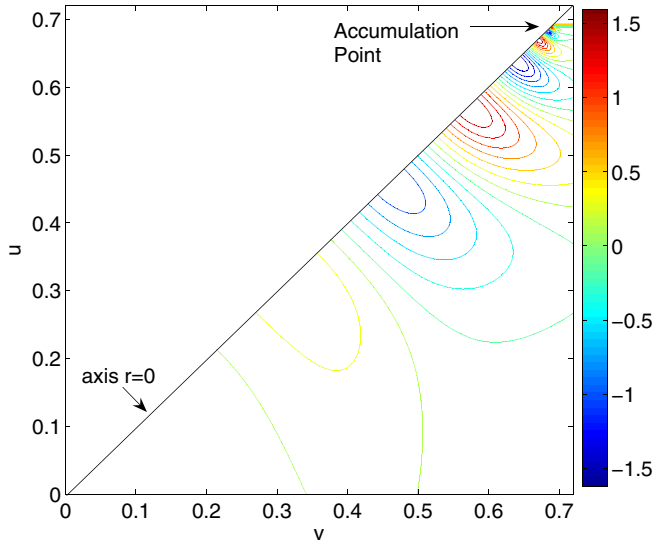

FIG. 2 (color online). $D = 6$: Contours of the scalar field profile in slightly subcritical collapse. After a short transient, the field oscillates, approaches the accumulation point where the curvature is maximal, and then disperses.

IV. RESULTS

In all dimensions that we examined, the near-critical collapse of the massless scalar field proceeds in a manner qualitatively very similar to the familiar 4D critical collapse. For $p < p_*$ the curvature along the axis grows, reaching some maximal value and then diminishes. In the strong curvature region the scalar field shows echoing on decreasing scales and subsequently disperses, see Fig. 2. In the supercritical collapse the field again rings but the curvature finally diverges and a black hole forms (the formation of an apparent horizon is signaled by e.g. the change of sign of g, which indicates that outgoing null rays are tilted back to smaller radii and do not escape to infinity).

In subcritical collapse we can define the "accumulation point" to be the location of maximal curvature.[5] We also label the proper time (10) of an on-axis observer at the accumulation point by T_*. In Fig. 3 we plot the scalar field on the axis as a function of $\log(T_* - T)$. After an initial transient the field becomes periodic in $\log(T_* - T)$, which is the attribute of DSS behavior in T. We were typically

[5]For the exactly critical solution it coincides with the singularity.

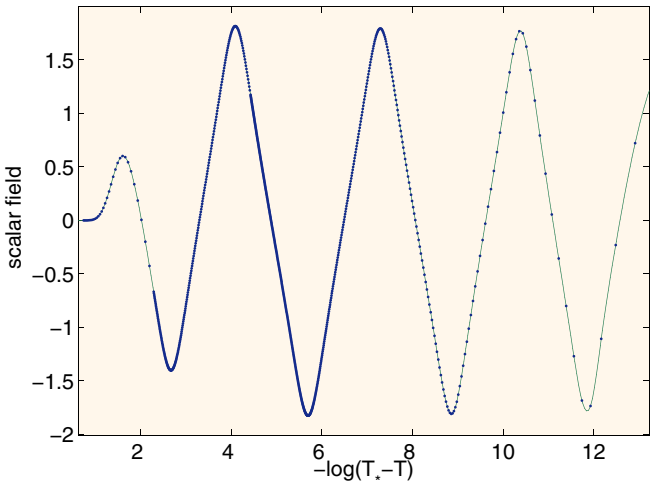

FIG. 3 (color online). $D = 5$: The scalar field on the axis as a function of $\log(T_* - T)$. The period of osculations is $\Delta \simeq 3.19$. The actual data is designated by points. The distance between the points increases close to T_* indicating the decrease of resolution.

able to observe about four full ringings of the scalar field in 4D and about three for higher D. From this data the oscillation period is computed, and so we get $\Delta(D)$.

Naturally, not only the scalar field is periodic, but other metric functions exhibit oscillations as well. In Fig. 4 we plot α at the axis. It shows twice the number of oscillation of the scalar field and decreases sharply on approaching the accumulation point. The evolution of the scalar curvature (9) along the axis is shown in Fig. 5 to oscillate with the same period as the scalar field. Since all variables are periodic, the quantity Δ can be derived from any one of them. We found that Δ's obtained from the various metric

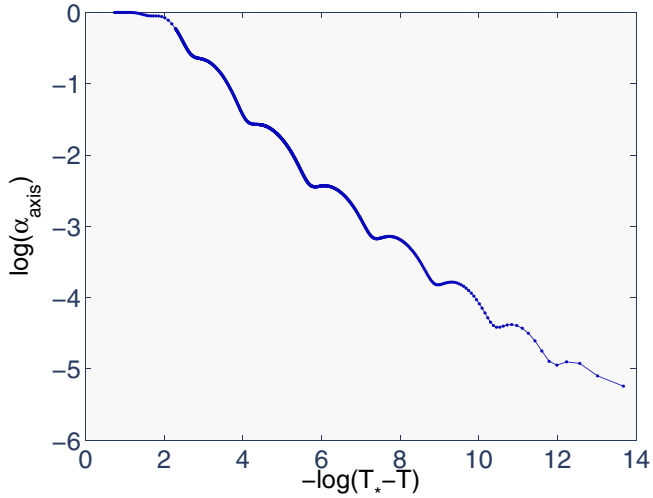

FIG. 4 (color online). $D = 5$: The metric function α on the axis decays fast as the accumulation point T_* is approached. Its evolution is accompanied by oscillations whose period ($\simeq 1.6$) is half the period of the scalar field ($\simeq 3.19$).

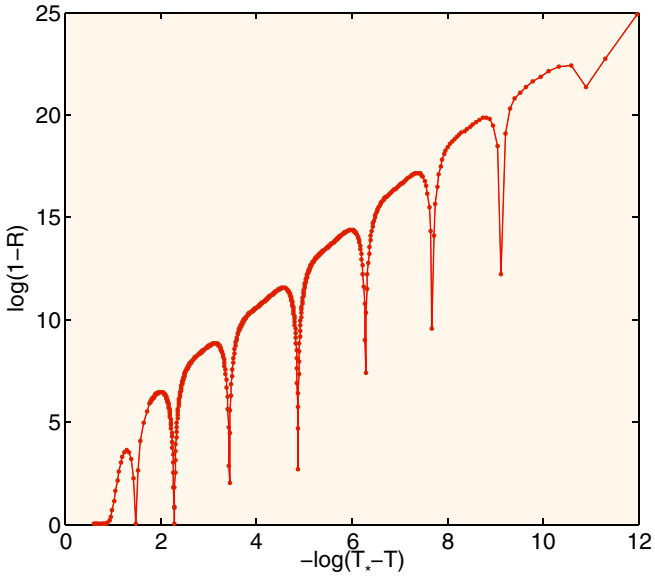

FIG. 5 (color online). $D = 7$: Behavior of the curvature as the accumulation point T_* is approached. The evolution of the curvature, like other metric functions, is accompanied by oscillations. After each pulsation $\log(1 - R)$ increases by Δ. The period of the last six echoes is approximately constant and equal to $\Delta/2 \simeq 1.41$. Similar behavior (with a different echoing period) is observed for other D's as well.

functions are consistent, see Table I for the values of Δ in the verified dimensions.

We evaluated the critical exponent γ from the behavior of the maximal curvature $R_{\max}$ in subcritical collapse, and

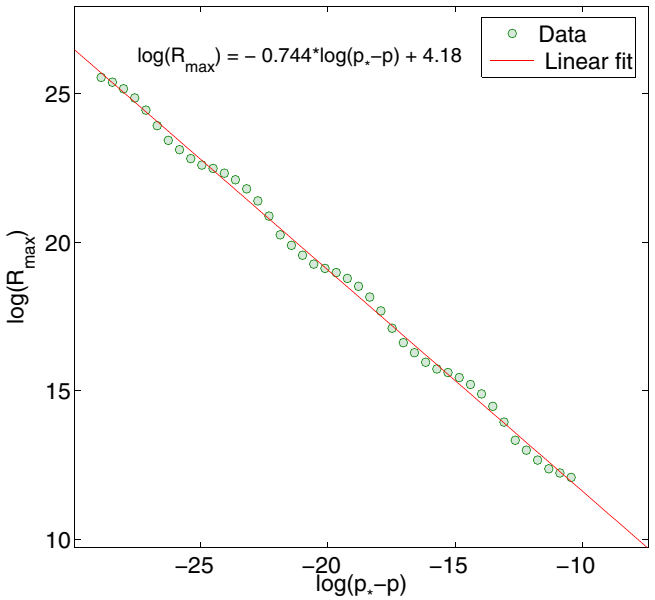

FIG. 6 (color online). $D = 4$: The maximal curvature on the axis as a function of $\log(p_* - p)$. The slope of the linear fit yields $\gamma = 0.372$ which agrees well with the value cited in the literature ($\simeq 0.374$).

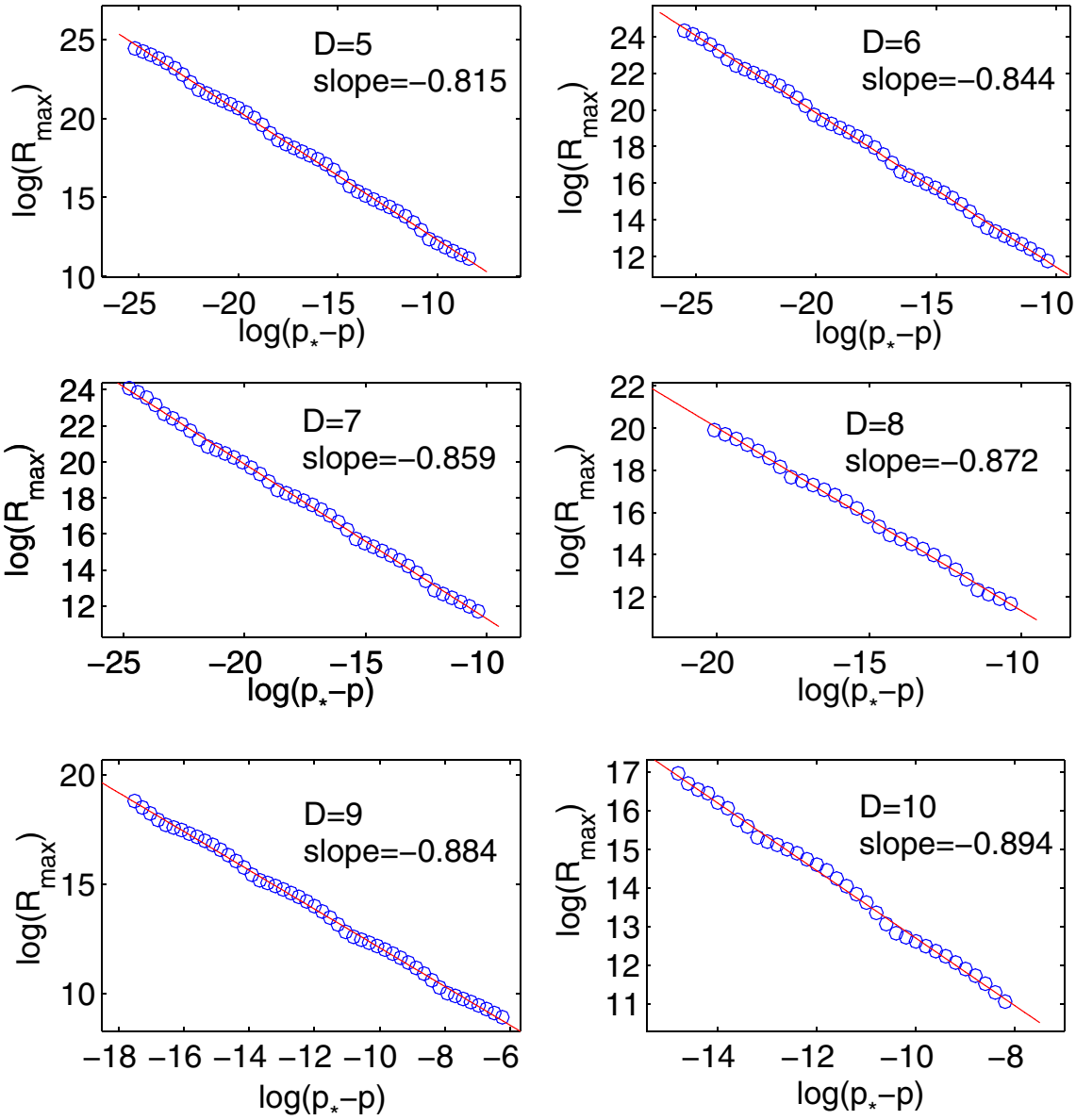

FIG. 7 (color online). The logarithm of the maximal curvature on the axis as a function of $\log(p_* - p)$ for different p's in various dimensions. The slope of the linear fit yields -2γ. Some wiggles, characteristic of the DSS solutions, occur about the linear fit.

not directly from the black hole mass scaling in supercritical collapse. The reason is that it is easier numerically to follow subcritical collapse than to estimate the black hole mass in supercritical collapse, because of difficulties in determining the position of the apparent horizon. (In addition, as we demonstrate below, it becomes increasingly difficult to find near-critical black holes in higher dimensions.)

For each dimension we examined the maximal curvature on the axis in several subcritical simulations. The result for $D = 4$ is plotted in Fig. 6 and the results for other D's are summarized in Figs. 7 and 8. It is evident from these plots that in all dimensions the maximal curvature has a dominant power-law scaling in $p_* - p$, with the exponent given by the slope of the linear fit in the figures. The critical exponent γ is then the minus half of value of the slope.[6] γ's for different dimensions are listed in Table I.

In addition to the dominant power-law scaling there are some residual "wiggles" or fine structure in the curvature's behavior, as can be seen in the figures. This was predicted for DSS solutions and explored in [19,20] where it was concluded that the "wiggling" period is $\Delta/(2\gamma)$. To illustrate this, we subtract from the measured $R_{\max}$ the dominant power-law dependence and plot the result for $D = 8$ in Fig. 9. By reflection about the horizontal axis the data is reorganized to have the doubled period. In all dimensions

[6]Recall, we define γ such that $|p - p_*|^\gamma$ has dimensions of length.

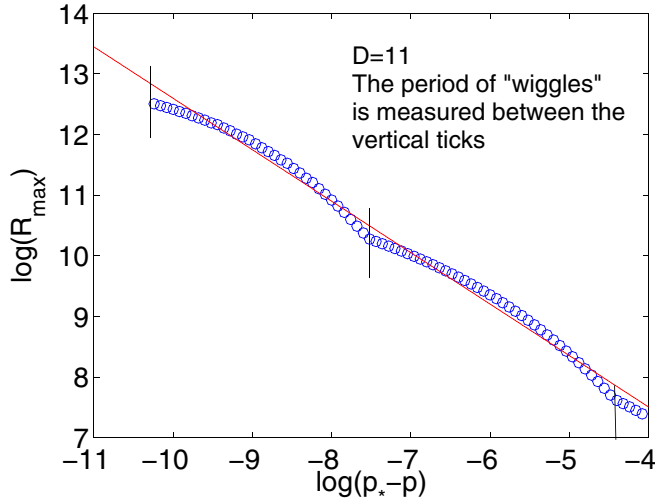

FIG. 8 (color online). The logarithm of the maximal curvature on the axis as a function of $\log(p_* - p)$ in 11D. Because of small number of wiggles and their large amplitude, the linear fitting approach fails to accurately estimate the slope. In this case we employ the fact that the period of wiggles ($\simeq 2.85$) is equal to $\Delta/(2\gamma)$ and use this to find $\gamma \simeq 0.44$ from the more accurate Δ. This approach is seen in lower dimensions to be consistent with the regular way to obtain γ.

we find the wiggling period to agree well with the theoretical prediction, Δ/γ. This is a nontrivial test for the numerically computed Δ and γ. Alternatively, since usually we can get Δ with somewhat higher precision, γ can be computed from the wiggles period. This is what we do in the $D = 11$ case because in this case the linear fitting approach does not yield a very accurate result, see Fig. 8.

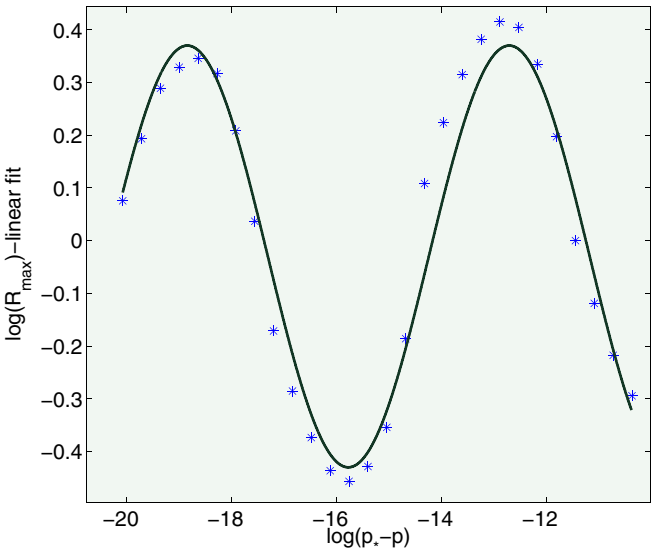

FIG. 9 (color online). $D = 8$: Normalized plot of $\log(R_{\max}) + 2\gamma \log(p_* - p)$ (stars) and a sine wave (solid line). The period of wiggles is about 6.18 and it agrees well with theoretical prediction $\Delta/\gamma \simeq 6.22$.

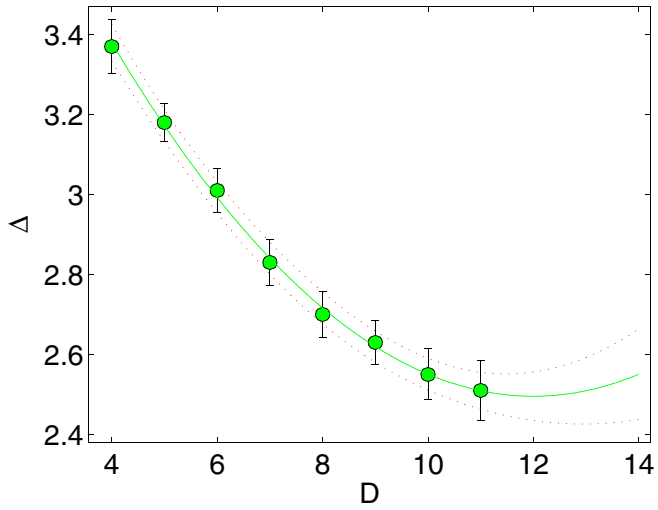

FIG. 10 (color online). Δ, including the errorbars, vs the spacetime dimension D. The solid line designates a second degree polynomial fitting, the dotted lines show the 95% prediction bounds. The speculative extrapolation to higher dimensions suggests that Δ reaches a minimum at $D \simeq 12$.

V. DISCUSSION

Let us now discuss the dimensional dependence of Δ and γ. We find that in the examined range of D's the echoing period $\Delta(D)$ is a decreasing function of dimension, as shown in Fig. 10. The observed dimensional dependence is well behaved in the sense that nothing in this plot forebodes that Δ will suddenly blow up. Assuming that this regularity continues (otherwise, a discontinuity in Δ will mark a phase transition) we add, in the same figure, a second order polynomial fitting and continue it slightly beyond the last data point. This *extrapolation* indicates that Δ might have a minimum[7] at about $D \simeq 12$.

Our computed $\gamma(D)$ increases up to $D \leq 10$ but for $D = 11$ it appears to decrease, although the errorbar is consistent with a constant or even slightly increasing value (see Fig. 11). This apparent decrease in γ might be due to a loss of numerical accuracy, but we are led to suspect the possibility that this is a true physical effect. This is suggested by the behavior of Δ. Let us analyze these two possibilities in more detail.

What could be the numerical cause for an underestimation of γ? In our scheme the threshold amplitude p_* can be obtained with somewhat decreasing accuracy as the dimension grows. Unfortunately our evaluation of γ relies heavily on the value of p_*; the abscissa in Figs. 6–8 is

[7]We do not address the details of this fitting since it has indicative aims only. Yet, one must bear in mind that the robustness of fitting is judged by the allowed variation of the fitting coefficients that still confines the fit within the errorbars. The proposed (quadratic) fit is significantly better in that sense than all other polynomial fits, making other behaviors than a minimum in Δ possible but less favored.

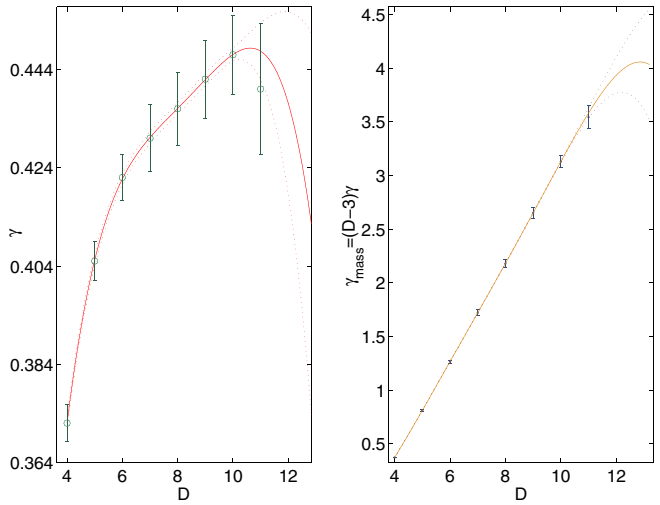

FIG. 11 (color online). γ and $\gamma_{\rm mass}$, with the errorbars, as a function of the spacetime dimension D. The dominant dimensional dependence of $\gamma_{\rm mass} = (D-3)\gamma$ is essentially linear increase due to the factor $D-3$, which masks the rather subtle variation of γ. The solid line designates a fourth order polynomial fit based on the data points in the range $4 \leq D \leq 10$ (the γ value for $D = 11$ is *not* used). The dotted lines show the 95% prediction bounds. The extrapolation for larger D's indicates the existence of a maximum somewhere in between $10 \leq D \leq 12$.

$-\log(p_* - p)$. Therefore, the quality of the linear fits in these figures and hence γ depends acutely on how well we estimate p_*. The effect is such that if the accuracy of p_* is lowered from one part in 10^{14} to one part in 10^{10} a few percents decrease in γ is induced. This might well be the reason we observe a downturn in $\gamma(D)$ at $D = 11$.

Having identified the possible cause for a numerical error in γ at $D = 11$, we can try to estimate this value independently of the numerical calculation at this dimension. To this end, we fit a polynomial (this time of fourth order) to γ using only data from $4 \leq D \leq 10$. By extrapolating this fit beyond the last ($D = 10$) data point we again observe a change in the trend: γ seems to reach a maximum at about $D = 11$ and then decreases. Remarkably, the numerically computed γ value at $D = 11$ complies with this extrapolated behavior. We tend to interpret this as a hint that the observed downturn in $\gamma(D)$ reflects the physical behavior of the system. This, as well as the behavior of $\Delta(D)$, marks the appearance of interesting and nontrivial dimensional dependence associated with critical collapse. (One might call the dimension where this occurs a "critical dimension.") If so, this intriguing phenomena clearly deserves better understanding.

While we stress that the allusion to the existence of a special dimension where the behavior of the echoing/scaling exponents changes are based on *extrapolation*, the phenomenon itself is not entirely unexpected. The Choptuik scaling, albeit in somewhat different circumstances, is conjectured to appear [14] in the black string/black hole system which does exhibit critical dimensions.[8] In that system, one considers black objects in a higher-dimensional spacetime with one compact dimension, $\mathbb{R}^{D-2,1} \times \mathbf{S}^1$. The known solutions are divided to black string solutions (whose horizon wraps the compact direction and so has the $\mathbf{S}^1 \times \mathbf{S}^{D-3}$ topology), and black hole solutions (with spherical, $\mathbf{S}^{D-2}$, horizon topology) localized on the circle. Consider the space of *static* solutions in this system. The different phases of solutions (black hole and black strings) are distinguished by an order parameter in this space, and the transition between these phases denotes a change in the topology of the solution. The local analysis [14] in the vicinity of the topology-changing (or merger) point shows that the geometry of the spacetime there should resemble a time-symmetric version of Choptuik's critical solution. Formally, the dilaton field g_{tt} plays the role of the scalar field in Choptuik's case, and the equations are the same. In both cases the problem is essentially two dimensional.

The similarity between these two systems lends insight into what happens near the merger point: the geometry here, as speculated in [14], is DSS and it resembles the Choptuik critical solution.[9] However, we would much prefer to have information on the dynamic solutions describing this phase transition. An attempt to trace the fate of an unstable string[10] in 5D was undertaken in [23,24], where it was shown that before the simulation crashes the black string becomes extremely nonuniform with a very long and thin neck. The numerical solution in [23,24] did not find any fine structure of the critical behavior near the pinch-off point. We believe that an improved code will discover that the behavior close to the pinching is similar to what happens in the axisymmetric near-critical collapse. In the latter case, evidence was given in [25] that a nonspherical mode appears causing bifurcations of the axisymmetric clumps of collapsing matter, which is reminiscent of the situation expected in the black string pinching.

In summary: we have obtained $\Delta(D)$ and $\gamma(D)$ for $4 \leq D \leq 11$ and found clues to the existence of a critical dimension where the behavior of these functions qualitatively changes. However, clues are still only that. It is important and interesting to improve the numerics and discover what really happens beyond $D = 11$. If extrema

[8]The critical dimensions in this system are (i) $D_{\rm merger} = 10$, above which the local geometry near the merger point argued to be conelike, and below which this conelike behavior is spontaneously broken[5,21], and (ii) $D_{\rm (second\ order)} = 13$ above which the phase transition becomes of second order [6,7].

[9]We note, however, that it is still not quite clear how to relate the Choptuik solution emerging in the collapse situation to its time-symmetric version studied in [14].

[10]It is known that a uniform black string becomes unstable [22] if "too thin." (Actually the relevant parameter is the ratio between the Schwarzschild radius of the string and the radius of the compact circle).

are present in the functions $\Delta(D)$ and $\gamma(D)$, what are the trends of these functions for even higher dimensions? Will they be discontinuous at some dimension, indicating a phase transition? Alternatively, if these functions are continuous will they tend towards some constant values? Perhaps Δ blows up at a certain dimension signaling that the solution ceases to be DSS and becomes continuously self-similar (conelike) beyond that dimension? We leave these questions open for future work, that will shed more light on this stimulating phenomenon.

ACKNOWLEDGMENTS

We thank Barak Kol for turning our attention to this problem, for many helpful discussions, and for sharing the results of his manuscript [14] prior to publication. E. S. is supported in part by an ISF grant.

[1] B. Kol, hep-th/0411240.
[2] R. C. Myers and M. J. Perry, Ann. Phys. (N.Y.) **172**, 304 (1986).
[3] R. Emparan and H. S. Reall, Phys. Rev. Lett. **88**, 101 101 (2002).
[4] B. Kol, hep-ph/0207037.
[5] B. Kol, hep-th/0206220.
[6] E. Sorkin, Phys. Rev. Lett. **93**, 031 601 (2004).
[7] B. Kol and E. Sorkin, Classical Quantum Gravity **21**, 4793 (2004).
[8] T. Damour, M. Henneaux, and H. Nicolai, Classical Quantum Gravity **20**, R145 (2003).
[9] M. W. Choptuik, Phys. Rev. Lett. **70**, 9 (1993).
[10] D. Garfinkle and G. C. Duncan, Phys. Rev. D **58**, 064024 (1998).
[11] C. Gundlach, Phys. Rep. **376**, 339 (2003).
[12] D. Garfinkle, C. Cutler, and G. C. Duncan, Phys. Rev. D **60**, 104007 (1999).
[13] M. Birukou, V. Husain, G. Kunstatter, E. Vaz, and M. Olivier, Phys. Rev. D **65**, 104036 (2002).
[14] B. Kol, hep-th/0502033.
[15] R. S. Hamade and J. M. Stewart, Classical Quantum Gravity **13**, 497 (1996).
[16] F. R. Tangherlini, Nuovo Cimento **27**, 636 (1963).
[17] M. J. Berger and J. Oliger, J. Comput. Phys. **53**, 484 (1984).
[18] D. Garfinkle, Phys. Rev. D **51**, 5558 (1995).
[19] C. Gundlach, Phys. Rev. D **55**, 695 (1997).
[20] S. Hod and T. Piran, Phys. Rev. D **55**, R440 (1997).
[21] B. Kol and T. Wiseman, Classical Quantum Gravity **20**, 3493 (2003).
[22] R. Gregory and R. Laflamme, Phys. Rev. Lett. **70**, 2837 (1993).
[23] M. W. Choptuik, L. Lehner, I. Olabarrieta, R. Petryk, F. Pretorius, and H. Villegas, Phys. Rev. D **68**, 044001 (2003).
[24] D. Garfinkle, L. Lehner, and F. Pretorius, Phys. Rev. D **71**, 064009 (2005).
[25] M. W. Choptuik, E. W. Hirschmann, S. L. Liebling, and F. Pretorius, Phys. Rev. D **68**, 044007 (2003).